The Journal of Navigation (2021), **74**:4 838–852
doi:10.1017/S0373463321000096

RESEARCH ARTICLE

Wireless power charging of drone using vision-based navigation

Swarnalatha Anumula,[1]* and Anitha Ganesan[2]

[1]Department of Aeronautical engineering, Tagore Engineering College, Chennai, India.
[2]Department of Aerospace Engineering, Madras Institute of Technology, Anna University, Chennai, India.
*Corresponding author. E-mail: swarnaramakanth@gmail.com

Received: 2 May 2020; **Accepted:** 5 February 2021; **First published online:** 25 March 2021

Keywords: charging pad, Raspberry Pi B+, supercapacitors, vision sensor, UAV

Abstract

For more efficient aerial surveillance, charging pads are set up at corresponding distances so that an unmanned aerial vehicle (UAV) can sustain its operations without landing. Usually manual intervention is required to land a UAV for charging and so extend its mission. To enable a UAV to operate autonomously, wireless power charging using inductive coupling is proposed. Using this method, the UAV's battery is charged until it reaches the next charging station. This paper focuses on two significant aspects of the process: vision-based navigation for charging pad detection, and wireless power charging. The coils were designed, and other parameters like mutual inductance, coupling coefficient and the distance between the coils for effective power transmission were analysed, using Ansys and Maxwell software. A quadcopter was built, with battery and Lidar sensor connected to the Arduino controller for low battery voltage detection and height measurement, respectively. Whenever the battery voltage is low, the UAV is steered towards the nearest charging pad using the global position navigation system. To test the process, the quadcopter was flown over the charging pad using a vision-based algorithm pre-defined in the image processor (Raspberry Pi B+).

1. Introduction

Unmanned aerial vehicles (UAVs), or drones, are used in the areas of surveillance, reconnaissance, target tracking, medical applications, logistics, combat operations, communications (Mahony and Kumar, 2012) and so on. However, the full potential of drone implementation continues to be limited by the restriction of battery life, as UAVs have to be charged at a ground station to continue the surveillance. Today, most electric drones have a battery life of 15–40 min. This relatively short battery life requires a drone to return to a fixed location, land, and power up for recharging or battery replacement. It requires a human being to charge the vehicle. The main reason for choosing vision-based navigation (Saripally et al., 2003) for detection of the charging pad is to allow the UAV to navigate accurately towards the target without human intervention and then to charge wirelessly. The camera serves as a vision sensor for vision-based navigation (Saripally et al., 2003). Vision sensors are low cost and capture an enormous amount of information. Vision sensors are passive; they do not get affected by any interference caused by the other sensors, i.e., light and audio sensors. As the battery needs a relatively long time to charge, a supercapacitor bank (Mukhopadhyay et al., 2018; Shah and Czarkowski, 2018) is used in tandem with the battery, as supercapacitors (Mukhopadhyay et al., 2018; Shah and Czarkowski., 2018) charge quickly.

This research explores the concept of wireless charging (Lu et al., 2015; Simica et al., 2015; Junaid et al., 2017; Jung et al., 2018) of a drone battery for continuous surveillance. Various wireless charging technologies are available (Valenti et al., 2007); among them inductive coupling is the best method

© The Royal Institute of Navigation 2021

https://doi.org/10.1017/S0373463321000096 Published online by Cambridge University Press

for small devices. Valenti et al. (2007) and Dale (2007) worked on autonomous recharging stations for drones using contact-based charging points. The drawback of this technique, however, is that the UAV has to bond with the electrodes exactly for recharging of the battery. Vicon Motion Systems (2016) investigated the use of position feedback control to land a UAV on a charging pad in an indoor environment. This technique has not been proven to work in an outdoor environment.

The global position navigation system (GPS) provides information about landing positions in the outdoor environment. However, it does not provide precise landing due to many factors, like wind, gust and so on. Vision-based guidance (Ahrens et al., 2009; Baik et al., 2011; Miguel et al., 2015) is required for the vehicle to move towards the charging point. Vision-based navigation provides accurate position information about the charging pad. Vision-based navigation has been used to detect a helipad (Lee et al., 2012). Vision-based target detection was implemented by a vertical takeoff and vertical landing UAV using Raspberry Pi as an image processor (Nyein et al., 2017).

The process of maximum power being transmitted wirelessly between the ground station and UAV with a strong coupling between transmitter and receiver was discussed in several researches. For transmitter to align with receiver, the hill climbing algorithm was proposed by Rohan et al. (2018). The power efficiency increases when there is resonance between the transmitter and the receiver. A few researchers have explained the strong magnetic resonance coupling (Kurs et al., 2007) and inductive resonance coupling (Han and Wentzloff, 2010) for wireless power transmission.

The objective of this paper is to develop UAVs for continuous surveillance purposes by using wireless power charging without human intervention. In the proposed method, the charging pad is identified by using a vision-based landing algorithm and the battery is autonomously charged. This work also provides a solution for long battery charging periods by incorporating supercapacitors with quick charging cycles. Section 2 focuses on the fundamentals of the UAV platform used in this work. Section 3 describes the principles of wireless power transfer, design and methodology. Section 4 describes charging pad detection. Section 5 describes the landing algorithm, and Section 6 presents the experimental results and discussions. The final section concludes the research work.

2. Theory and design considerations

To show autonomous landing features and wireless power charging, a quadcopter was built from scratch, as shown in Figure 1. A state-of-the-art Pixhawk flight controller is used to control the quadcopter in the air. The quadcopter is equipped with a GPS receiver, Lidar sensor, Arduino controller and an image processor (Raspberry Pi). The vision sensor (camera) is attached to the image processor (Raspberry Pi) to detect the charging pad. The Lidar unit measures height by illuminating the target with laser light. Both Lidar sensor and battery (by using potential divider) are connected to the Arduino controller. The Arduino controller thus simultaneously knows the battery voltage and the height of the quadcopter with respect to the ground. This information is transmitted to the ground station computer by using an HC12 module. The Raspberry Pi communicates with the ground station computer using inbuilt Wi-Fi. The supercapacitors are also called double-layer capacitors. The capacitance of these capacitors is very high. In this work, four 500 F, 3 V supercapacitors are connected in series to achieve a total voltage of 12 V. The specifications of the quadcopter are shown in Table 1 below.

3. Wireless power transfer

This section presents the essential working principles of the wireless power transfer. Wireless power transfer (Zhang et al., 2013) utilises several technologies for transmitting energy through electromagnetic fields. The wireless charging methods are classified as near-field and far-field charging. This research focuses on near-field charging, by using inductive wireless power charging (Lu et al., 2015). Far-field techniques are not feasible because antennas and other electronic equipment add load to the UAV. The transmitter circuit is placed on the ground station, and the receiver coil is attached to the vehicle. The wireless charging circuit is implemented on the printed circuit board, three transmitter coils are placed on

https://doi.org/10.1017/S0373463321000096 Published online by Cambridge University Press

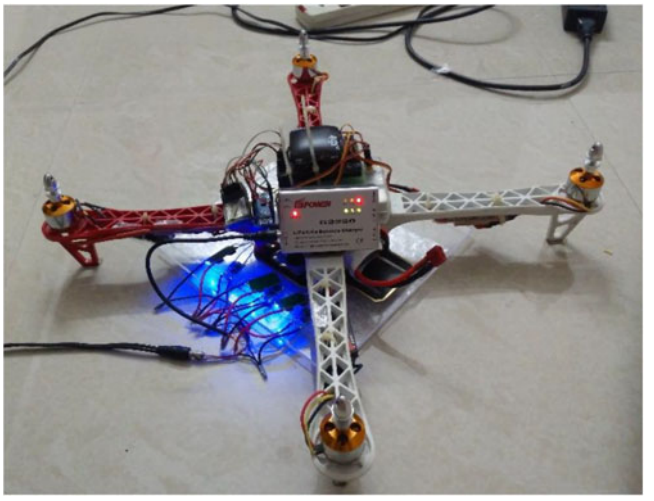


Figure 1. *Quadcopter.*

Table 1. *Quadcopter specifications.*

S. no	Specifications
Frame	F450 composite frame
Flight controller	Pixhawk
Radio fly	Fly Sky transmitter and receiver
Battery	2200 mah, 11·1 V 3S LiPo
Image processor	Raspberry Pi B+
Camera	Logitech B425
GPS	3DR Neo 7M
Power module	3DR power module
ESC	Wolfpack 30A (Bel Heli) ESC
Motors	2212 1000 KV brushless DC
Propeller	9343 DJI self-locking (CW/CCW)
Supercapacitors	500 F, 3 V
RP Lidar	A1M8

the ground station and three receiver coils connected to the bottom of the vehicle for wireless charging of the battery. The design uses a DC power source to charge the aerial vehicle. Since inductors do not work with DC, an oscillator is used to change DC to AC. However, this AC signal is weak and cannot be used to transfer power to the aerial vehicle. Hence a power amplifier is used. Commercial power amplifiers are costly; therefore a simple MOSFET amplifier is used to amplify the power. The IRF 510 power amplifier can handle a current of 3 A and voltages up to 30 V; hence it is suitable for this application. Coils are powered by the power amplifier and an alternating magnetic field is produced, which induces an opposing electromagnetic field in the secondary coils. The receiver provides an alternating frequency; hence a rectifier is used to convert the AC to DC. A power regulator is incorporated (LM7805 IC) to regulate the fluctuations in the system to control the output to 5 V. The DC output produced by each of the receiver coils is connected in series to satisfy the requirements of the charger and connected to a DC male power adapter. For minimum losses, coil design is crucial and the coupling coefficient, magnetic flux distribution and Q factor have to be considered. The coil design mainly depends on the number of

https://doi.org/10.1017/S0373463321000096 Published online by Cambridge University Press

turns and method of winding the coil. The coil design is analysed by using Ansys Maxwell software and a single input–single output model is selected for wireless charging.

D represents the distance between the two coils. Let W denote the resonant frequency of the two coils.

$$W = \frac{1}{\sqrt{L1C1}} = \frac{1}{\sqrt{L2C2}} \tag{1}$$

where $L1, L2$ = self-inductance of transmitter and receiver coils, and $C1, C2$ = resonant capacitance of transmitter and receiver coils.

$$\left(RS + RT + JWL1 + \frac{1}{JWC1}\right) IT + JWMIR = VS \tag{2}$$

$$JWMIR + \left(RL + RR + JWL2 + \frac{1}{JWC2}\right) IR = 0 \tag{3}$$

where RS and RL denote the impedances at the source of the transmitter, and the load on the receiver (Lu et al., 2015). The resistances of the transmitter and receiver coils (Lu et al., 2015) are denoted by R_T and R_R, respectively. The received power at the load of the receiver is as follows

$$P2 = P1Q1Q2\eta1\eta2k^2(D) \tag{4}$$

where $P1$ is the power at the source of the transmitter. $\eta1$ and $\eta2$ represent the efficiencies of the transmitter and receiver, respectively, which are calculated as

$$\eta1 = \frac{RS}{RS + RT} \tag{5}$$

$$\eta2 = \frac{RL}{RL + RR} \tag{6}$$

$Q1$ and $Q2$, the quality factors of the transmitter and receiver, are provided by

$$Q2 = \frac{WL2}{RT + RS} \tag{7}$$

$$Q1 = \frac{WL1}{RL + RR} \tag{8}$$

and k denotes the coupling coefficient factor (Lu et al., 2015) between the two coils.

$$k = \frac{M}{\sqrt{L1L2}} \tag{9}$$

If the radii of the transmitting and receiving coils and the distance between them is known, the coupling coefficient is given by the following function,

$$k^2(D) = \frac{r1^3 r2^3 \pi^2}{(D^2 + r1^3)^3} \tag{10}$$

By substituting Equation (10) in Equation (4), the power at the receiving coil can be found.

$$P2 = P1Q1Q2\eta1\eta2\frac{r1^3 r2^3 \pi^2}{(D^2 + r1^3)^3} \tag{11}$$

The design uses three small inductance coils, instead of a single inductor, to reduce interference between the on-board microcontroller and the sensors such as magnetometer, gyroscope, accelerometer and GPS modules. If a single coil is used, the effect is so high that the power distribution board present in

https://doi.org/10.1017/S0373463321000096 Published online by Cambridge University Press

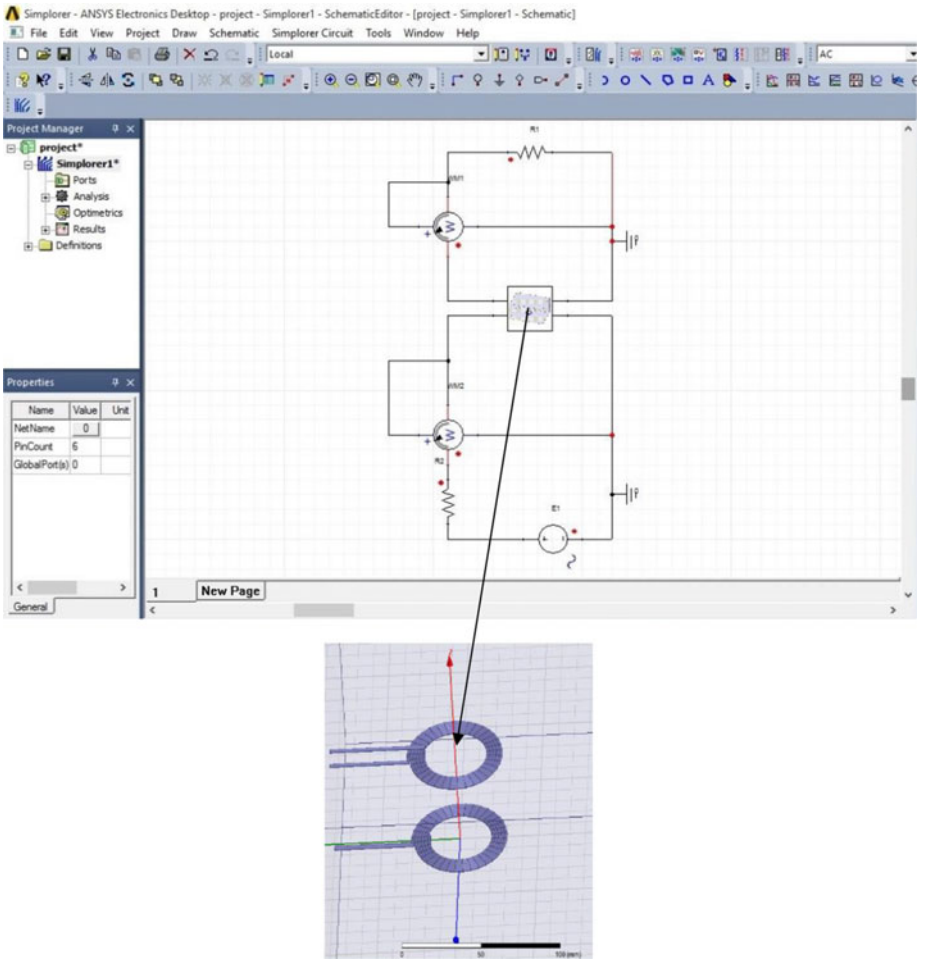


Figure 2. *Coil design model of single input–single output in Ansys and Simplorer software.*

the UAV can produce stray potential because of changing magnetic flux by Faraday's laws of induction, which can cause devastating after-effects to the circuits present in the system. The design considerations also limit the maximum radius of the coils to 5·5 cm. Figure 2 presents the coil design with a diameter restricted to 5·5 cm, and the single input–single output circuit is implemented in Ansys and Simplorer software. Variation of the coupling coefficient to distance is also analysed.

An analysis has been carried out for the peak power transfer efficiency of different frequencies and for various separation distances of the transmitter and receiver coils. From this analysis, the best working frequency of the coils is determined. The graph in Figure 3(a) presents the power transfer efficiency with frequency. The maximum power efficiency occurs at a frequency of 25 MHz. When the distance increases, the coupling coefficient is reduced, as shown in Figure 3(b). Based on the results, the ideal value of the distance between the coils was chosen for maximum power transmission.

Figure 3(a) shows that the maximum power transfer efficiency occurs at a frequency of 25 MHz. Minimum power transfer efficiency occurs at frequencies of 5 MHz and 50 MHz. The bandwidth of the radiation pattern can be increased if the distance between the coils is reduced. So the absolute bandwidth between transmitter and receiver coil can be given by

$$\text{Bandwidth} = F_H - F_L \tag{12}$$

https://doi.org/10.1017/S0373463321000096 Published online by Cambridge University Press

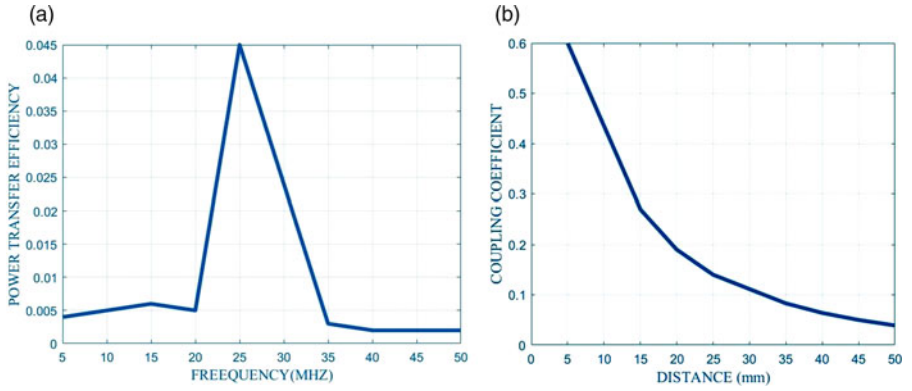


Figure 3. *(a) Variations of power transfer efficiency with frequency, (b) variations of coupling coefficient with distance.*

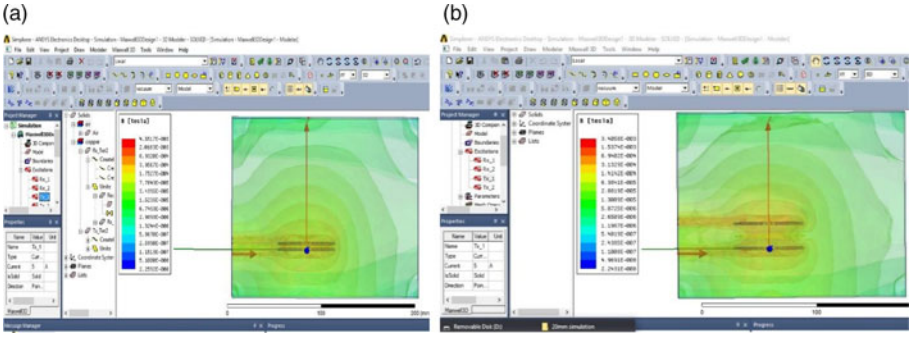


Figure 4. *Magnetic field distribution for (a) 5 mm, (b) 20 mm.*

Figure 4 describes the magnetic field distribution for a separation distance from 5 mm to 20 mm. It can be seen that when separation distance between coils increases, the flux coupled with coil decreases. The maximum power transfer occurs when the distance between the coils is the minimum possible. So, when the quadcopter flies very near to the charging pad, the magnetic flux distribution between the coils will be at its maximum.

4. Charging pad detection

The proposed algorithm for vision-based detection is shown in Figure 5. The vision-based target detection is implemented on Raspberry Pi 3 in the image pre-processing stage. The first step is to convert the video acquired from the Raspberry Pi camera into frames. In the image pre-processing stage, bilateral and media filters are applied to remove the noise from the image. An adaptive threshold is applied to separate the foreground from the background. Hough circle transform is used to detect the target in the image, and by using image moments centroid is found. The horizontal distance between the reference image centroid and the actual image centroid is estimated. The distance error is given as an input signal to the proportional derivative and integral (PID) controller, and gains are tuned manually. When the distance error becomes zero, the quadcopter is exactly on the target, and the controller gives the landing command to hover on the target for wireless charging.

The charging pads are placed at pre-defined locations, as shown in Figure 6. The vehicle identifies the charging pad's location based on GPS location, hovers over it, and is charged wirelessly. Whenever the battery is being charged, the 'disarm' command is given from the ground station to the Arduino to disarm the motors. Once the battery and supercapacitors are partially charged, then arming the vehicle

https://doi.org/10.1017/S0373463321000096 Published online by Cambridge University Press

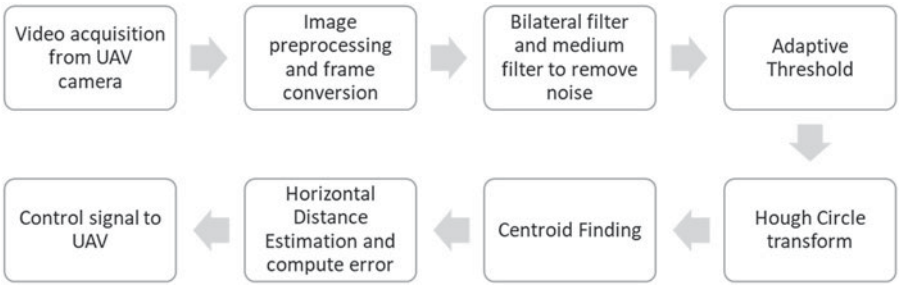


Figure 5. *Proposed vision algorithm.*

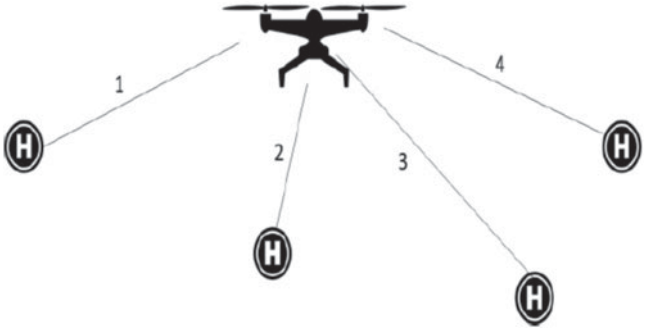


Figure 6. *Helipads at various locations.*

Algorithm

Step 1: Get the current location of the drone.
Step 2: Get the GPS position of all charging pads.
Step 3: Calculate the drone's present position.
Step 4: Calculate the distance between the drone and all the charging pads using the Haversine function.
Step 5: Find the nearest charging pad.
Step 6: Follow the waypoints until the charging pad detected by the vision-based algorithm.
Step 7: Hover over the pad until the battery is charged to at least 50%.

causes the motors to spin. Throttle down position, and right rudder position is held for 5 s. Because of this procedure, battery power is saved, and the endurance of the vehicle increases.

5. Method for landing

The flow diagram for the landing loop shown in Figure 7 is explained in this section. The process happens at two locations simultaneously, one at the image processing station and the other at the flight controller. These two processes combined together provide a unique and definitive output. Initially, the quadcopter powers up its motors directly, with no connection to the flight controller and Raspberry Pi, which allows the system to compensate for the initial power drop during the boot-up process. In this work, mission planner software is used to visualise the data from the flight controller board. The telemetry module is used to send and receive the commands. The image processing computer, i.e., Raspberry Pi B+, is

https://doi.org/10.1017/S0373463321000096 Published online by Cambridge University Press

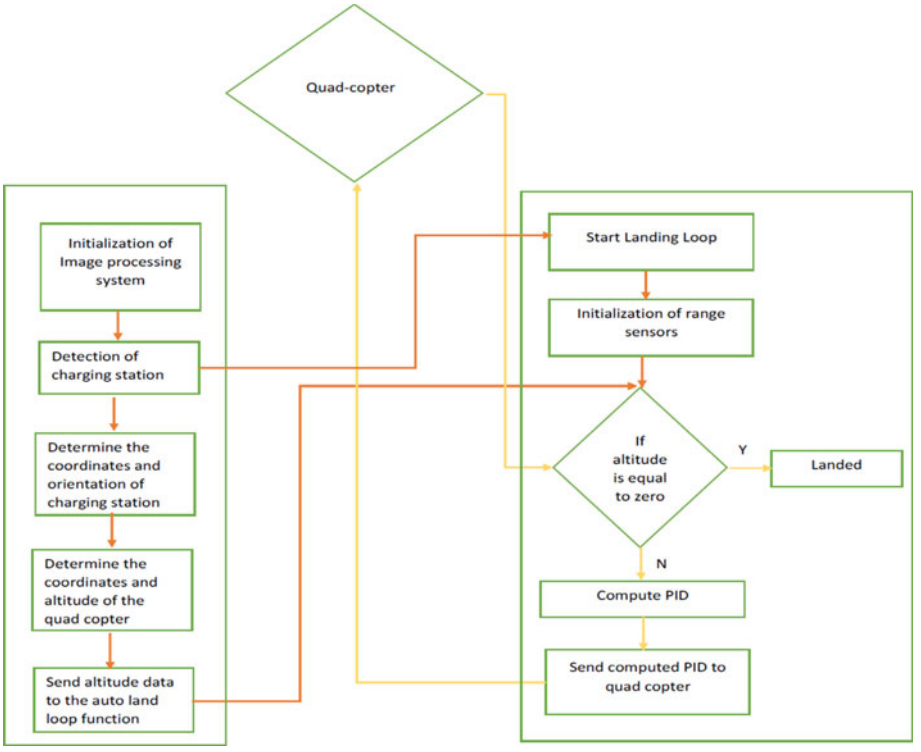


Figure 7. *Flow diagram for the landing loop.*

powered up through the power lines from the telemetry port. Once both the systems start to operate, it can arm the quadcopter. The Raspberry Pi is connected to the internet via a Wi-Fi module present on it. The wireless connection to the image processing computer triggers main code to initialise the camera. Once the charging pad is detected, the altitude (height) of the quadcopter from the charging pad is determined and is displayed to the user via ssh client software. Raspberry Pi also sends this altitude along with the respective pulse width modulation (PWM) signal to land and the quadcopter's flight controller helps in safe landing. Once the quadcopter has successfully landed, the user receives a message at the ssh display on a remote desktop or a mobile phone. When the flight controller receives the 'land' command PWM signal from Raspberry Pi, it starts the landing loop. In the landing loop, the controller locks the current GPS coordinates of the current position and maintains the position of the quadcopter to a stable level, so it does not steer away in the air due to external gusts. Then the throttle is retarded sufficiently using a machine learning (ML) algorithm pre-defined in the code of the Pix hawk flight controller. The ML algorithm, based on the previous landing, determines the required PID values to run the landing loop of the system and also adapts to the current environment of the quadcopter, thus always maintaining a stable landing. The landing loop, based on predetermined as well as current conditions, sets the PID values. From these PID values, the PWM throttle signal is required to land the quadcopter at a constant descent velocity. When the descent velocity is lower than the required value, less throttle is sent to the motors, which causes the quadcopter to descend at an increasing rate. This sophisticated algorithm runs internally on the quadcopter. This process lands the quadcopter in the desired location, showing an automated landing.

The proposed image processing algorithm is checked in the simulation environment using software packages such as MATLAB and XPLANE maker. The vehicle is modelled with planemaker tool. The design of the quadcopter began with an initial estimation of the size of a UAV. Length of the arm is chosen in accordance with the diameter of the propeller of the vehicle. The diameter of the engine is

https://doi.org/10.1017/S0373463321000096 Published online by Cambridge University Press

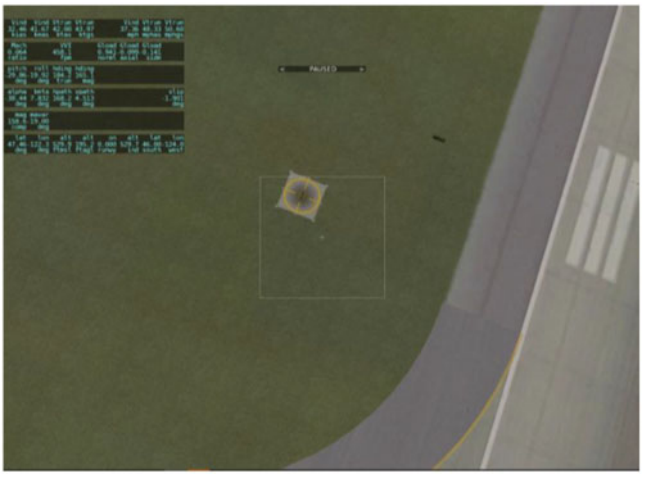


Figure 8. *UAV approaching the landing target with various locations in simulation.*

determined as a function of the engine speed. The motors are cross-mounted and the UAV fuselage designed as required. Landing gear is placed at the bottom of each engine to maintain the centre of gravity and balance of the vehicle. The simulation is then done in MATLAB using the SIMULINK block set tools. In this simulation, the deflection of the control area is transformed into engine RPM as required. The controller used for the pitch and roll channel is a PID controller with automated tuning based on the input and output data. The vehicle approaches the target using vision-based navigation, as illustrated in the simulation in Figure 8.

6. Experimental results

This section discusses the experimental results of wireless charging and the autonomous landing of a UAV on a charging pad using vision-based navigation.

6.1. Wireless power charging

The module was tested with an input voltage of 18 V and a power supply unit 1 A, and the output voltage was determined using a multimeter. The module produces a power of 5·34 V with a separation distance of 5 mm. The wireless power transfer (WPT) module can handle loads up to 1·3 A, so by connecting three modules in series would produce sufficient voltage to provide the input power to the LiPo balance charger module. The receiver module with three coils is attached to the base of the quadcopter, as shown in Figure 9(a). The transmitter modules are placed on the ground, as shown in Figure 9(b), for real-time testing. Figure 10 illustrates an experimental test bed for WPT. The circuit is tested using 15 W lights. The waveforms of the input transmitter and the output receiver are tested with a cathode ray oscilloscope. The transmitter and receiver are resonant and visualised using a cathode ray oscilloscope. The circuit is implemented on the printed circuit board.

6.2. Lidar calibration and height measurement

The Lidar sensor is connected with a computer using a USB adopter, and Slamtech Robostudio is used to take the angle and distance information of the object. The test is conducted by keeping the obstacle at a distance of 1 m, as shown in Figure 11. Lidar scan data when the object is placed at a distance of 1 m is shown in Figure 12.

https://doi.org/10.1017/S0373463321000096 Published online by Cambridge University Press

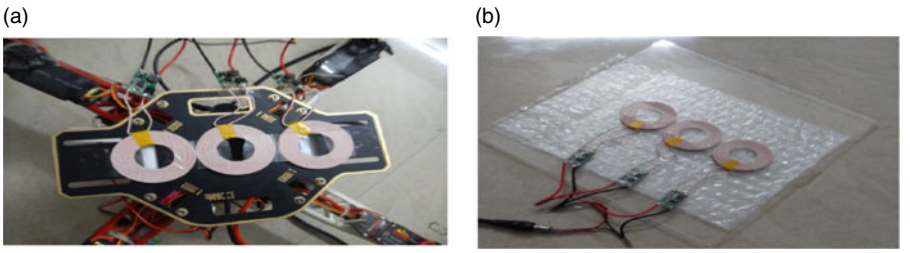


Figure 9. *(a) Transmitter module, (b) receiver modules.*

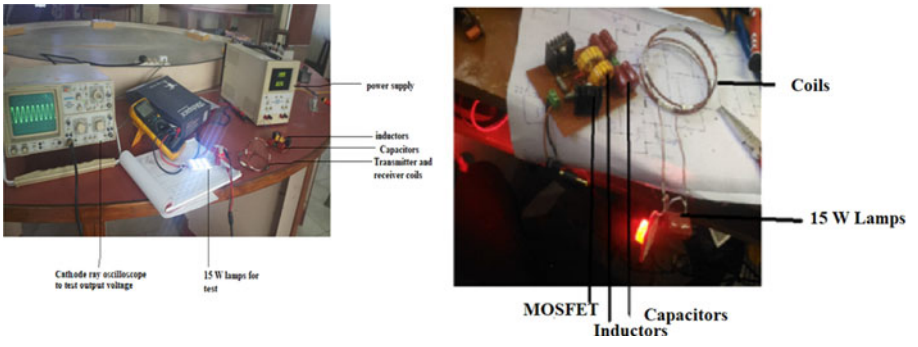


Figure 10. *WPT experimental setup.*



Figure 11. *Lidar sensor setup for calibration in the indoor environment.*

The root mean square value of the obstacle kept at 1 m is 1·011 m. The sensor can be calibrated to provide accurate distance.

Figure 13 illustrates the Arduino controller used for distance (height) and battery voltage measurement. The Lidar sensor measures distance to a landing pad by illuminating it with laser light and measuring the reflected light with a sensor. The battery is connected to the Arduino through the potential divider network. The program is pre-defined in the Arduino board and connected to the ground station by using an HC-12 transmitter and receiver module. The battery voltage and distance are monitored continuously in the ground station. Whenever the battery voltage is low, the landing command is given from the ground station to search for a charging pad.

6.3. Landing pad detection.

When several points that fall on the perimeter are known, the Hough transform is used to find the parameters of a circle. For a circle with centre (a, b) and radius R, the equation of the circle is specified

https://doi.org/10.1017/S0373463321000096 Published online by Cambridge University Press

#Angle	Distance (M)
0.9338	0.9999
1.4996	1.002
2.0764	0.999
2.6367	0.999
3.2025	0.999
3.7793	1.004
4.3396	0.999
4.9054	1.003
5.4822	1.001
6.026	1
6.5918	1.003
7.1521	1.001
7.7179	1.005

Figure 12. *Lidar scan data when object is placed at a distance of 1 m.*

by (Rhody and Carlson, 2005)

$$r^2 = (x-a)^2 + (y-b)^2 \tag{13}$$

$$x = a + r\cos\theta, y = b + r\sin\theta \tag{14}$$

When the angle θ sweeps through the full 360-degree range, the points (x,y) trace the perimeter of a circle. The centroid of a shape is the arithmetic mean (i.e., the average) of all the points in a shape. Each shape is made of pixels, and the centroid is the weighted average of all the pixels making up the shape. The centroid is given by the formula (Rhody and Carlson, 2005):

$$C = \frac{1}{n}\sum_{i=1}^{n} x^i \quad C_x = \frac{M_{10}}{M_{00}} \quad C_y = \frac{M_{01}}{M_{00}} \tag{15}$$

where C_x is the coordinate of X, C_y are the coordinates of Y and M is the image moments (Wikipedia, Image moments).

$$M_{pq} = \sum_{p}\sum_{q} x^p y^q I(x,y)\ \ p,q = 0,1,2\ldots.. \tag{16}$$

where $I(x,y)$ is the pixel intensity.

The Euclidean metric is the straight-line distance between two points in Euclidean space. The Euclidean distance between points 'p' and 'q' is the length of the line segment connecting them. For two dimensions, where $p = (p_1, p_2)$ denote the centroid coordinates and $p = (q_1, q_2)$ denotes the image centre:

$$d(p,q) = \sqrt{(q_1 - p_1)^2 + (q_2 - p_2)^2} \tag{17}$$

Mean absolute error measures the average magnitude of the errors in a set of predictions, without considering their direction. Mean absolute error was calculated and found to be 0·21 cm, 1·40 cm and 2·13 cm for a horizontal distance of 30 cm, 45 cm and 60 cm, respectively. Several experiments were conducted with the landing pad at a fixed height, at 430 cm, 630 cm and 830 cm, and the landing pad image was taken at different horizontal locations, at 10 cm, 20 cm, 30 cm, 45 cm and 60 cm. The error

https://doi.org/10.1017/S0373463321000096 Published online by Cambridge University Press

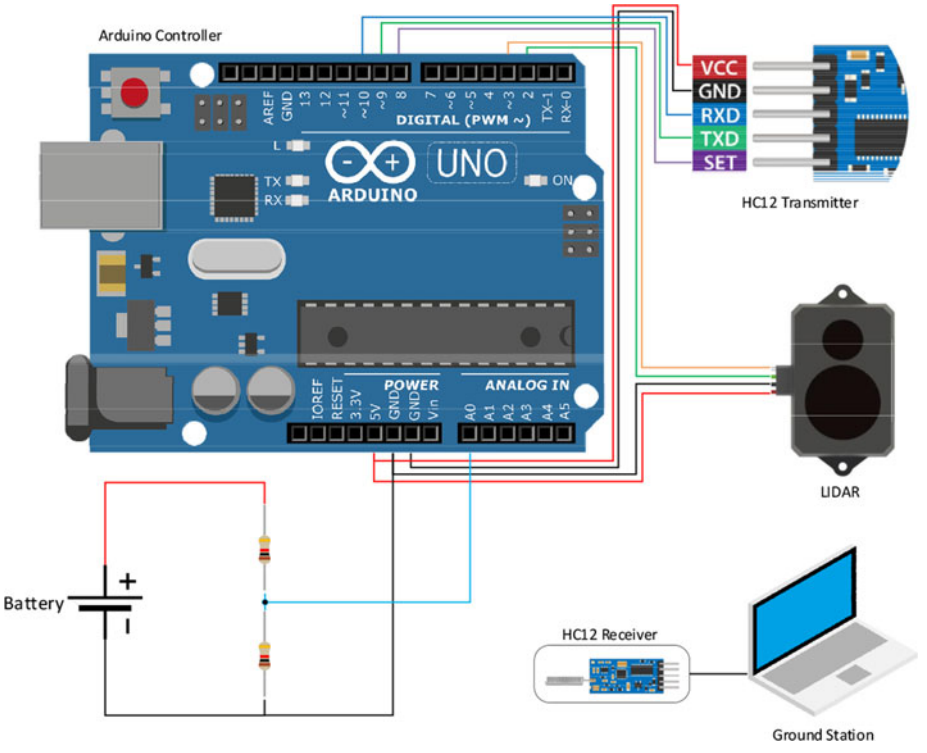


Figure 13. *Arduino controller for distance and battery voltage measurement.*

Table 2. *Error between the measured and actual value of horizontal distance.*

S. no	Horizontal distance (cm)	Measured horizontal distance (cm)	Mean absolute error (cm)
1	30	30	0
2	30	20·2	9·8004
3	30	26·755	3·2451
4	30	34·41	−4·41
5	30	28·949	1·051
6	30	18·279	11·721
7	30	26·038	3·9618
8	30	35·396	−5·396
9	30	30	0
10	30	20·2	9·8004
11	30	26·755	3·2451
12	30	34·41	−4·41

between measured horizontal distance and actual horizontal distance, with 30 cm height, is shown in Table 2.

$$\text{MAE} = \frac{\sum_{i=1}^{n} |y_i - x_i|}{n} \tag{18}$$

The UAV detects the landing pad and tracks it by using a vision-based algorithm, as shown in Figure 14. The video is converted into frames and the centroid location is also identified. The quadcopter

https://doi.org/10.1017/S0373463321000096 Published online by Cambridge University Press

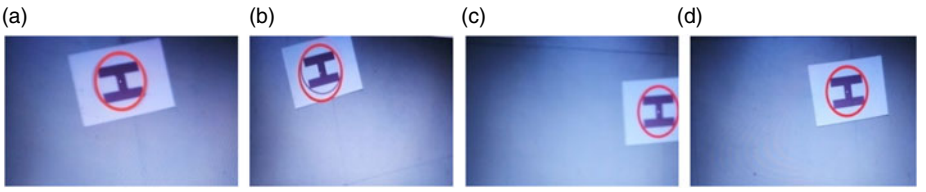


Figure 14. *Quadcopter using a vision algorithm to detect helipad: tracking frames (a) 10th frame, (b) 20th frame, (c) 50th frame, (d) 100th frame.*

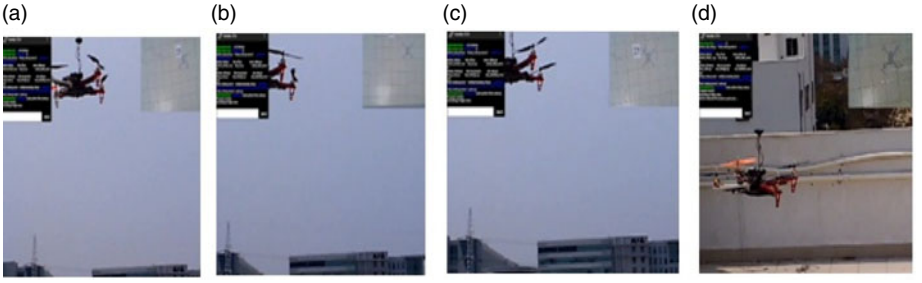


Figure 15. *Quadcopter using a vision algorithm, tested in real time: (a) 30th frame, (b) 50th frame, (c) 75th frame, (d) 100th frame.*

Table 3. *Power efficiency comparison.*

S. no	Year	Power efficiency (%)
1	Current work	87%
2	Junaid et al. (2017)	75%
3	Zhang et al. (2013)	46·4%

was tested in real time using a vision-based algorithm; the video of the test was converted into frames, as shown in Figure 15.

6.4. WPT efficiency

This section describes the results of power transfer efficiency using WPT. The input voltage is set to 18 V, the output voltage at 15·8 V and load current at 1·3 A. In this work, three coils are connected in series. Efficiency is calculated by the ratio of output to input power. The module is tested with an input voltage of 18 V and 1 A power supply unit, and the output voltage is determined. The module produces an output of 5·34 V at a separation distance of 5 mm. Hence, it is suitable for this model. The WPT module handles loads up to 1·3 A, by connecting three modules in series, which produces sufficient voltage required to provide the input power to the LiPo balance charger module. This proposed solution gives an efficiency of an average of 87%. The efficiency of WPT is good and workable for the proposed application of this research. The efficiency was computed using the ratio of the output power and the input power as follows.

$$E = \frac{Po}{pi} \times 100 \tag{19}$$

The maximum reported efficiency (Junaid et al., 2017) was 75% with input voltage set at 16 V and output voltage at 12·42 V, and an average efficiency (Zhang et al., 2013) of 46·4%. The proposed solution gives an efficiency of an average of 87% as compared with previous work, as shown in Table 3.

https://doi.org/10.1017/S0373463321000096 Published online by Cambridge University Press

7. Conclusion

In this work, near-precision landing of a UAV on the charging pad is attempted using image processing technology. The transmitter is assembled at the ground station, and the receiver coils are arranged on the aerial vehicle, in a fashion which does not hinder the operation of the on-board sensors and flight control modules. Tests were carried out with the above setup, and charging was accomplished using the module. Mean absolute error was calculated and found to be 0·21 cm, 1·40 cm and 2·13 cm for a horizontal distance of 30 cm, 45 cm and 60 cm between UAV and charging pad, respectively. The simulation was conducted with many iterations (7–8) for tuning of controlled constants. The proposed solution gives an efficiency of an average of 87% as compared with previous work.

8. Future work

In future precision landing can be attempted by using upgraded hardware and software, to control the quadcopter and land precisely at a minimal circular probability error. The charging stations can be assembled on rooftops or remote towers and transmit their location to modern autopilot systems installed within the UAV to enable it to navigate to the desired location autonomously.

Acknowledgements. The authors acknowledge the support rendered by the Division of Avionics, Department of Aerospace Engineering, Madras Institute of Technology, Anna University, Chennai.

References

Ahrens, S., Levine, D., Andrews, G. and Jonathan, P. (2009). Vision-Based Guidance and Control of a Hovering Vehicle in Unknown GPS-Denied Environments. *2009 IEEE Proc. Int. on Robotics and Automation, Kobe International Conference Center*, Kobe, Japan, 12–17 May. doi:10.1109/ROBOT.2009.5152680.

Baik, K., Shin, J., Ji, S., Shon, W. and Park, S. (2011). A Vision System for UAV Position Control, *Proc. IEEE Aerospace 2011*. doi:10.1109/AERO.2011.5747515.

Dale, D. R. (2007). Automated ground maintenance and health management for autonomous unmanned aerial vehicles. Master's thesis, Massachusetts Institute of Technology, Cambridge, MA, USA.

Han, S. and Wentzloff, D. D. (2010). Wireless Power Transfer Using Resonant Inductive Coupling for 3D Integrated I.C.s. *Proc. Inc.* IEEE *International 3D Systems Integration*, Munich, Germany, *16–18 November 2010*; 1–5.

Junaid, A. B., Konoiko, A. and Zweiri, Y. (2017). Autonomous wireless self-charging for multi-rotor unmanned aerial vehicles. *Energies*, **10**, 803. doi:10.3390/en10060803

Jung, S., Lee, T., Mina, T., Kartik, B. and Ariyur, K. (2018). Inductive or Magnetic Recharging for Small UAVs, *SAE International*. 27 August 2018. doi:10.4271/2012-01-2115.

Kurs, A., Karalis, A., Moffatt, R., Joannopoulos, J. D., Fisher, P. and Soljac, M. (2007). Wireless power transfer via strongly coupled magnetic resonances. *Science*, **317**, 83–86.

Lee, S., Jang, J.-W. and Baek, K.-R. (2012). Implementation of Vision-Based Real Time Helipad Detection System, *Proc. Int. on Control, Automation and Systems*, Oct. 17–21, 2012 in ICC, Jeju Island, Korea. Available at: https://ieeexplore.ieee.org/document/6393429/metrics.

Lu, X., Wang, P., Niyato, D., Kim, D. I. and Han, Z. (2015). Wireless charging technologies: Fundamentals, standards, and network application. *IEEE Communications Surveys, and Tutorials*. doi:10.1109/COMST.2015.2499783.2015. Available at: https://www.arxivvanity.com/papers/1509.00940.

Mahony, R. and Kumar, V. (2012). Aerial robotics and the quadrotor. *IEEE Robotics & Automation Magazine*, **19**, 19.

Miguel, A., Mendez, O., Kannan, S. and Voos, H. (2015). Vision Based Fuzzy Control Autonomous Landing with UAVs: From V-REP to Real Experiments, *2015, Proc. 23rd Mediterranean on Control and Automation (*MED*)*, 16–19 June 2015, Torremolinos, Spain. doi:10.1109/MED.2015.7158723.

Mukhopadhyay, S., Fernandes, S., Shihab, M. and Waleed, D. (2018). Using small capacity fuel cells onboard drones for battery cooling: An experimental study. *Applied Science*, **8**, 292. pp. 2–16. doi:10.3390/app8060942.

Nyein, E., Tun, H. M., Naing, Z. M. and Moe, W. K. (2017). Implementation of vision-based landing target detection for VTOL UAV using Raspberry Pi. *International Journal of Science & Technology Research*, **6**(4), ISSN 2277-8616, 184–188.

Rhody, H. and Carlson, C. F. (2005). Hough circle transforms, Oct 11, 2005.

Rohan, A., Rabah, M., Talha, M. and Kim, S.-H. (2018). Development of intelligent drone battery charging system based on wireless power transmission using hill climbing algorithm. *Applied System Innovation*, **1**, 44. doi:10.3390/asi1040044.

Saripally, S., Montgomery, J. F. and Sukathme, G. S. (2003). Vision based autonomous landing of unmanned aerial vehicle. *Robotics and Automation*, **3**, 2799–2804. Available at: https://www.eecis.udel.edu/~cer/arv/readings/paper_saripalli.pdf.

Shah, N. and Czarkowski, D. (2018). Supercapacitors in tandem with batteries to prolong the range of UGV systems. *MPDI Electronics*, 2–12. doi:10.3390/electronics7010006.

https://doi.org/10.1017/S0373463321000096 Published online by Cambridge University Press

Simica, M., Bila, C. and Vojisavljevicb, V. (2015). Investigation in wireless power transmission for UAV charging. *Procedia Computer Science*, **60**, 1846–1855. doi:10.1016/j.procs.2015.08.295

Valenti, M., Dale, D., How, J., Pucci de Farias, D. and Vian, J. (2007). Mission Health Management for 24/7 Persistent Surveillance Operations. *Proc. AIAA Guidance, Navigation, and Control and Exhibit*, Hilton Head, SC, USA, 20–23 August 2007.

Vicon Motion Systems Ltd. (2016). Available at: http://www.vicon.com/ [Accessed April 2016].

Zhang, J., Li, Y., Qiao, G. and Li, Z. (2013). Battery swapping and wireless charging for a home robot system with remote human assistance. *IEEE Transactions on Consumer Electronics*, **59**, 747–755.

Cite this article: Anumula S, Ganesan A (2021). Wireless power charging of drone using vision-based navigation. *The Journal of Navigation* **74**: 4, 838–852. https://doi.org/10.1017/S0373463321000096

https://doi.org/10.1017/S0373463321000096 Published online by Cambridge University Press